A Novel Load Flow Algorithm for Islanded AC/DC Hybrid Microgrids

Mohammed Elsayed Nassar, *Student Member, IEEE*, Amr A. Hamad, *Student Member, IEEE*, M. M. A. Salama, *Fellow, IEEE*, and Ehab F. El-Saadany, *Fellow IEEE*

***Abstract*—This paper proposes a novel branch-based load flow approach for isolated hybrid microgrids. This evolving network configuration involves the application of a distinctive operational philosophy that poses significant challenges with respect to conventional load flow techniques. Hybrid microgrids are characterized by small-rating, droop-based distributed generators (DGs) and by variable but coupled frequency and dc voltage levels. In particular, the absence of a slack bus that results from the small DG rating impedes the application of traditional techniques such as branch-based methods. To overcome these limitations, a modified branch-based approach provided the basis for the development of the proposed algorithm. The new algorithm solves the load flow sequentially by dividing the problem into two coupled ac and dc subproblems. The coupling criterion is established by modeling and updating the power exchange between the subgrids, hence enabling an accurate and efficient formulation of the subproblems. For each subproblem, a modified directed forward-backward sweep has been developed to perform the load flow analysis based on consideration of the individual characteristics of each subgrid. Case study results demonstrate that the algorithm is applicable and effective for the steady-state analysis of several operational factors associated with an isolated hybrid microgrid system: 1) load changing; 2) converter outages; and 3) the probabilistic nature of renewable generation and loads.**

***Index Terms*—Droop-based DGs, forward-backward sweep, hybrid ac/dc microgrids, islanded microgrids, load flow.**

I. Introduction

THE RECENT penetration of distributed generation (DG) into the existing electricity grids and the consequent development of active distribution networks (ADNs) have prompted an exploration of power distribution in a dc microgrid paradigm.

Compared to traditional ac networks, dc microgrids offer numerous advantages: 1) greater system efficiency due to the lower number of conversion stages required for connecting electronic and nonlinear loads; 2) more cost-effective accommodation of energy storage and dc-based DG units, such as solar photovoltaic (PV), type-4 wind turbines, and fuel cells; 3) more efficient and compatible platform for dc loads, such as dc LED lights and plug-in electric vehicles (PEVs); 4) less interference with ac grids because of the absence of synchronization problems; 5) more flexible energy paradigm for future expansion [1].

A number of dc networks have already been established as expansions of conventional ac distribution systems [2], and a new hybrid configuration of ac and dc subgrids is considered to be viable in the near future [3]. The installation of distributed generators (DGs) within such hybrid distribution systems could provide highly reliable service because the load supply to different ac and dc subgrids is maintained even in the case of interruptions at the main substation. In islanded operation mode, reliability would be reinforced by the implementation of droop characteristics. This feature would coordinate the DG output power in a decentralized manner [4].

In an ac subgrid, the DGs employ the appropriate system frequency and voltage droops, enabling the active and reactive power of the subgrid, respectively, to be shared. Similarly, the DGs adapt the system voltage in order to share the load power in the dc subgrid. At the same time, the interlinking converter (IC) between the ac and dc subgrids works to equalize the loading levels of the ac and dc subgrids by relating the ac frequency to the dc voltage [5]–[7].

The coupling between the ac frequency and the dc voltage is a unique feature of hybrid microgrids. Such coupling enables both ac and dc subgrids to share the overall loading without the presence of a slack bus in either subgrid. This operational scheme incurs variations in system frequency and voltage level with changes in the system loading. Since load and generation are always balanced by the primary control, the implementation of a noncritical secondary control with minimum communication requirements will suffice. The secondary control maintains the system frequency and voltage at levels very close to the nominal values and also achieves additional operational objectives [8].

The practical application of this operational philosophy to large-scale hybrid microgrids necessitates a profound

Manuscript received October 11, 2016; revised January 29, 2017, May 16, 2017, and September 19, 2017; accepted October 23, 2017. Date of publication November 10, 2017; date of current version February 18, 2019. Paper no. TSG-01392-2016. *(Corresponding author: Mohammed Elsayed Nassar.)*

M. E. Nassar is with the Department of Electrical and Computer Engineering, University of Waterloo, Waterloo, ON N2L3G1, Canada, on leave from the Faculty of Engineering, Electrical Department, Alexandria University, Alexandria 21526, Egypt.

A. A. Hamad is with the National Research Council Canada (NRC-CNRC), Ottawa, ON K1A 0R6, Canada, on leave from the Faculty of Engineering, Department of Electrical Power and Machines, Cairo University, Giza 12613, Egypt.

M. M. A. Salama is with the Department of Electrical and Computer Engineering, University of Waterloo, Waterloo, ON N2L3G1, Canada.

E. F. El-Saadany is with the Department of Electrical and Computer Engineering, University of Waterloo, Waterloo, ON N2L3G1, Canada, on leave from Petroleum Institute, Khalifa University of Science and Technology, Abu Dhabi, UAE.

Color versions of one or more of the figures in this paper are available online at http://ieeexplore.ieee.org.

Digital Object Identifier 10.1109/TSG.2017.2772263

understanding of system behavior. Such understanding must be acquired from comprehensive steady-state analysis for a variety of loading and generation levels. An accurate and reliable load flow algorithm is thus essential for the performance of a number of planning and operational studies. These studies include, but are not limited to, an examination of DG allocation and sizing, VAr planning and control, optimum power management, and protection design and contingency analysis [8]–[10]. Several load flow algorithms have been proposed for multi-terminal dc systems (MTDCs), which are hybrid ac/dc systems at the transmission level. However, these formulations are unsuitable for microgrids because of the key features that characterize islanded ac/dc microgrids and distinguish them from MTDCs: frequency variations, coupling between the ac and dc variables, and the lack of a slack bus.

For distribution systems, load flow problem is formulated and solved through either derivative-based algorithms (Newton's method) or derivative-free algorithms (branch-based methods). Derivative-based techniques were originally developed for large and meshed networks. The necessity of following a standard format was a crucial factor that prompted the application of derivative-based methods for droop-regulated microgrids. For example, Newton-Raphson approaches have been adopted for solving both ac and hybrid ac/dc microgrids.

On the other hand, derivative-free methods offer more reliable and superior performance for distribution systems due to several intrinsic features: a high number of nodes, a radial topology, and a high (R/X) ratio of feeders [11], [12]. Since these factors contribute to the ill-conditioned behavior of large distribution systems, they may hinder the convergence of some conventional derivative-based algorithms. In contrast, forward-backward methods guarantee robust convergence for radial distribution networks. They also offer advantages for solving large-scale networks such as: simplicity of implementation, system-independent convergence time, and low computational and memory requirements [13]. Although these methods were primarily developed for radial distribution systems, the employment of a multi-port compensation routine has extended their application to include weakly-meshed networks [14], [15]. The first derivative-free algorithm to solve load power flows in islanded microgrids is proposed in [16]. Based on BF current sweeps, this algorithm has an inner loop for frequency updating and an outer loop for global voltage correction in order to overcome the challenge of the absence of a slack bus. Díaz *et al.* [16] stipulated that good starting points are required if their algorithm is to achieve reasonable convergence, and they proposed approximate expressions for such points.

This paper introduces a novel branch-based load flow algorithm developed for performing steady-state analysis in hybrid ac/dc microgrids. In this algorithm, the traditional branch-based load flow approach has been adapted to accommodate the unique features and challenges of islanded hybrid microgrids. Such features include variable frequency, droop-controlled DGs, interaction between ac and dc subgrids, and the lack of a slack bus. Unlike the Newton-based methods applied in [17] and [18], the proposed algorithm has inherited the intrinsic features of branch-based techniques so that the algorithm is inversion and derivative free.

The proposed algorithm first decomposes the load flow problem for the hybrid system into two interlinked smaller subproblems for the ac and dc subgrids, and then solves them sequentially. This approach reduces problem complexity, and thus offers an enhanced performance speed without compromising the solution efficiency. For the decomposition process, the coupling between the ac frequency and the dc voltage is still maintained, i.e., the dc subgrid is modeled as a constant-power DG at the point of common coupling (PCC) on the ac side.

A novel branch-based load flow algorithm, named the forward-return-forward-backward sweep (FR-FBS) has been created for solving the ac subgrid. The proposed algorithm alternates between FB and BF to allow inter-iteration updating of the solution variables, thus improving the convergence. In addition, the ac load flow is based on power sweeps rather than current sweeps. The effect of the ac subgrid is also modeled and reflected on the dc side as a reference bus whose voltage is a function of the ac subgrid frequency.

A backward-forward sweep (BFS) algorithm has been developed for solving the islanded dc subgrid and determining the power interchange between the dc and ac subgrids. This BFS is a directed load flow solution that starts with an exploration and categorization of the subgrid nodes and branches in order to set the direction of the solution. Like the BFS of the dc subgrid, the FR-FBS also begins with an exploration and categorization of the ac subgrid nodes and branches in order to set the solution direction. These two algorithms are then integrated to form the hybrid load flow tool to be used with islanded hybrid microgrids. This paper makes the following contributions:

1) A simple and derivative-free algorithm is proposed for solving the power flow of islanded hybrid microgrids. The algorithm is based on a branch-based technique with active and reactive power sweeps.
2) A novel interplay between the well-known concepts of sweeping forward and backward is introduced. This action improves algorithm performance through inter-iteration updating of the solution variables.
3) A novel representation of the dc subgrid and its effect on the ac-subgrid frequency is proposed and used for the inter-iteration frequency updating.
4) A quadratic equation for the modeling of dc droop-regulated DGs is formulated for solving the BFS load flow in dc subgrids.
5) A probabilistic load flow tool is introduced. The tool is created by integrating the proposed load flow algorithm with the probabilistic models of load and renewable generation. This tool is employed for studying the operation of islanded hybrid microgrids supplied from a mix of renewable-based and droop-controlled DGs.

The remainder of the paper is organized as follows. Section II introduces the problem description along with the hierarchy of the proposed load flow algorithm. The directed FB load flow for the ac subgrid is explained in Section III, and the BFS for the dc subgrid is presented in Section IV. The integration of both algorithms for the formulation of the sequential

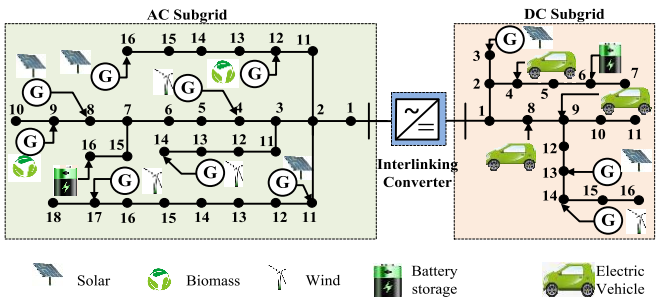

Fig. 1. Layout of a hybrid microgrid.

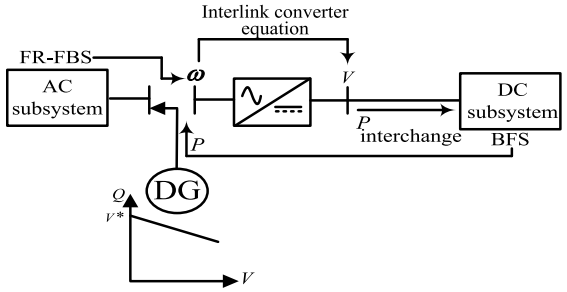

Fig. 2. Solution hierarchy of the hybrid system.

hybrid load flow tool is set out in Section V. Section VI describes the case studies conducted to validate the algorithms, and Section VII concludes the paper.

II. Problem Description and Solution Hierarchy

In general, a hybrid microgrid consists of islanded ac and dc subgrids connected by an IC, as illustrated in Fig. 1. To meet load demand in each subgrid, the main DG strategy is to implement droop characteristics. For the ac subgrid, the DG units meet the active and reactive power load requirements through the implementation of P/ω and Q/V droop characteristics. For the dc subgrid, they implement P/V droop characteristics to meet the active power demand.

At the same time, the IC between the subgrids is responsible for sharing the overall load demand of the hybrid paradigm, regardless of the location of the load. The ICs achieve this objective by transferring active power from lightly loaded subgrids to heavily loaded ones. It is important to note that the loading condition of a subgrid is inferred through a different variable for each subgrid: the frequency in the ac subgrid and the voltage in the dc one. An IC must therefore map these variables into a common normalized range in order to quantify the loading conditions of both the ac and dc subgrids:

$$\omega_{pu} = \frac{\omega - 0.5(\omega_{max} + \omega_{min})}{0.5(\omega_{max} - \omega_{min})} \tag{1}$$

$$V_{pu} = \frac{V_{dc,i} - 0.5\left(V_{dc,max} + V_{dc,min}\right)}{0.5\left(V_{dc,max} - V_{dc,min}\right)} \tag{2}$$

where ω_{max} and ω_{min} are the respective maximum and minimum values for the permissible frequency of the ac subgrid, and $V_{dc,max}$ and $V_{dc,min}$ are the respective maximum and minimum allowable voltages in the dc subgrid.

In this formulation, the loading condition has been normalized between -1 and 1 for both the ac and dc subgrids. However, other normalizing ranges could be applied according to operator preference. An IC could thus transfer an appropriate amount of active power to equalize the normalized values [5]:

$$\omega_{pu} = V_{pu} \tag{3}$$

Equation (3) represents the coupling between the ac and dc subgrids, and thus indicates that the ac and dc load flows are also coupled. In other words, the solution cannot be applied to each subgrid individually, due to the mutual coupling between the subgrids. Instead, branch-based load flow algorithms can be developed for solving each subgrid independently while the other subgrid is modeled according to this criterion. The forward-backward sweep (FBS) for solving hybrid ac/dc systems is thus formulated as the integration of the FR-FBS load flow developed for the ac subgrid, and the BFS load flow created for the dc subgrid (Fig. 2).

The dc subgrid is represented as an ac DG unit at the ac subgrid with a constant power $P_{interchange}$ and a $Q - V$ droop [5]. On the other hand, the dc subgrid has a reference bus with a constant voltage V calculated from the ac subgrid frequency ω. The calculation is based on the operation of the IC expressed in (1) to (3) [5]. The ω calculated for the ac subgrid determines the computation of the value of V for the dc subgrid. The load flow in the dc subgrid can then be solved to find $P_{interchange}$.

The next step is to establish the load flow in the ac subgrid. The change in ac frequency ($\triangle\omega$) related to the active power mismatch $\triangle P$ can be calculated and the frequency updated accordingly. The same sequence is repeated until convergence. The load flows in the ac and dc subgrids are formulated as branch-based load flows. These flows and their integration to form the hybrid load flow algorithm are described in detail in the following sections.

III. FR-FBS for the AC Subgrid

A modified FBS algorithm is used for solving the load flow in the isolated ac subgrid. It is worth mentioning that only balanced ac subgrids are considered in his work to highlight the solution methodology; however, this work can be augmented with negative and zero sequence load flow subroutines for solving unbalanced microgrids. The proposed algorithm has a primary forward sweep calculation that starts from a fixed point and follows a main path. The algorithm incorporates the interplay between the forward-backward calculations at any emanating branches. The next stage is a return to the starting point to repeat that step but with the incorporation of the updated version of some variables. The algorithm derives its designation as FR-FBS from this flow. The branch-based load flow equations and the FR-FBS are presented in this section.

A. Load Flow Calculations

The active and reactive branch load flows are used for the load flow sweeps. For the simple two-bus system shown in Fig. 3, in the backward sweep, (4)-(9) are used for calculating the active and reactive line flows between the two successive

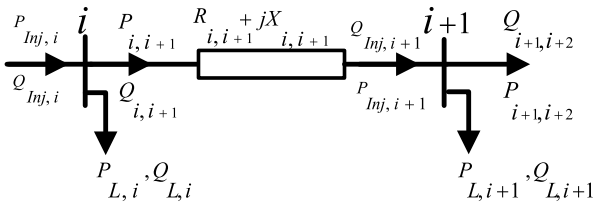

Fig. 3. Simple two-bus ac system.

buses (i and i+1). The calculations are based on the voltage magnitude of the starting bus (i.e., bus i+1), the line impedance, the microgrid frequency, and the loading of the starting bus. In contrast, in the forward sweep, (11)-(15) are used for calculating the bus voltage magnitude and angle, given the active and reactive line flows and the voltage magnitude at the starting bus (i in this case).

$$P_{i,i+1,k} = P_{Inj,i+1,k} + P_{Loss(i,i+1,k)} \tag{4}$$

$$Q_{i,i+1,k} = Q_{Inj,i+1,k} + Q_{Loss(i,i+1,k)} \tag{5}$$

$$P_{Inj,i+1,k} = P_{i+1,i+2,k} + P_{L,i+1,k} - P_{gAC,i+1} \tag{6}$$

$$Q_{Inj,i+1,k} = Q_{i+1,i+2,k} + Q_{L,i+1,k} - Q_{gAC,i+1} \tag{7}$$

$$P_{Loss(i,i+1,k)} = R_{i,i+1}\frac{\left(P_{Inj,i+1,k}\right)^2 + \left(Q_{Inj,i+1,k}\right)^2}{\left|V_{i+1,k}\right|^2} \tag{8}$$

$$Q_{Loss(i,i+1,k)} = \omega_{cor,k}X_{i,i+1}\frac{\left(P_{Inj,i+1,k}\right)^2 + \left(Q_{Inj,i+1,k}\right)^2}{\left|V_{i+1,k}\right|^2} \tag{9}$$

$$\omega_{cor,k} = \frac{\omega_k}{\omega^*} \tag{10}$$

$$\left|V_{i+1,k}\right| = \sqrt{\left|V_{i,k}\right|^2 - 2\beta + \left|I_{i,i+1,k}\right|^2\left|Z_{i,i+1,k}\right|^2} \tag{11}$$

$$\beta = R_{i,i+1}P_{i,i+1,k} + \omega_{cor,k}\, X_{i,i+1}Q_{i,i+1,k} \tag{12}$$

$$\left|I_{i,i+1,k}\right|^2 = \frac{\left(P_{i,i+1,k}\right)^2 + \left(Q_{i,i+1,k}\right)^2}{\left|V_{i,k}\right|^2} \tag{13}$$

$$\left|Z_{i,i+1,k}\right|^2 = \left(R^2{}_{i,i+1} + \left(\omega_{cor,k}X_{i,i+1}\right)^2\right) \tag{14}$$

$$\delta_{i+1,k} = \delta_{i,k} + tan^{-1}\frac{R_{i,i+1}Q_{i,i+1,k} - X_{i,i+1}\omega_{cor,k}P_{i,i+1,k}}{\beta}. \tag{15}$$

B. FR-FBS Algorithm

The FR-FBS load flow for isolated ac microgrids is employed in the load flow problem for the ac subgrid. The problem is solved starting from an arbitrary point, termed the pivot point, and using an FR-FBS directed toward a point called the reflection point. At this point, the system frequency and voltage are updated according to the active and reactive power mismatch calculations, respectively. Following this updating, the algorithm returns to the pivot point with an updated voltage and again starts a directed FR-FBS from the pivot point.

The sequence of FR-FBSs continues until the active and reactive power mismatches become negligible. The FR-FBS load flow process starts with an exploration of the system and the classification of the buses (points) and lines into appropriate categories. The system points are categorized as follows:

1) *Reflection point:* Any leaf load point can be selected as a reflection point, but only one reflection point is selected for the system. The active and reactive power mismatches are calculated at this point.
2) *Pivot point:* This term refers to any point with a droop-controlled DG, but only one point is selected as the pivot.
3) *Leaf point:* This point is the terminal point of a line, expressed as follows:

$$i \in Leaf \ iff \sum_{j=1,j\neq i}^{N} A_{ij} = 1 \ \forall j \in N. \tag{16}$$

4) *Joint point:* This point joins more than two lines, as follows:

$$i \in Joint \ iff \sum_{j=1,j\neq i}^{N} A_{ij} > 2 \ \forall j \in N \tag{17}$$

where A is the network connectivity matrix, and $A_{ij} = 1$ if nodes i and j are interconnected.

Network lines, on the other hand, are classified as one of the following three types of network sections:

1) *Branch section:* a line that starts at a leaf point and ends at a joint point
2) *Main trunk section:* a line that starts at a joint point and ends at a joint point or at the point directly connected to the reflection point
3) *Pivot branch section:* a line that starts at the pivot point and ends at a joint point

After the network lines and buses have been classified, the FR-FBS is directed and executed through the application of the algorithm outlined in the pseudo-code shown in Fig. 4. As indicated in Fig. 4, the flow of the FR-FBS solution is directed through the ac subgrid according to the previously defined network line and point categories. Dijkstra's shortest path algorithm [19] was adopted for this algorithm as a means of determining the shortest path between any selected point and the reflection point. Dijkstra's algorithm is applied when this information is needed for directing the solution flow, as explained in the next section. Any other algorithm for finding the shortest path can be used, but whichever shortest path algorithm is selected will be run just once at the categorization stage.

C. Algorithm Description

The 21-bus system depicted in Fig. 5 illustrates the functioning of the algorithm. The system points are assigned as follows:

1) *Reflection point:* {0}
2) *Pivot point:* {18} (or any other DG point)
3) *Leaf points:* {8,11,14,18,21}
4) *Joint points:* {4,7,13,16}

Based on this point designation, the network lines are divided into the following sections:

1) *Main trunk sections:* {1-2-3-4, 4-5-6-7, 4-12-13 and 13-15-16}

FR-FBS algorithm for ac subgrid

1 Input Network data $(z_{i,j}, A_{i,j}, N)$
2 Input DG data $(N_{dg}, m_{p,i}, m_{q,i}, Q_{i,max}, V^*, \omega^*)$
3 Set $Pflow_{i,j,0}$, $Qflow_{i,j,0}$ to zero
4 Categorize the network points and lines
5 $k \leftarrow 1$
6 Calculate the initial $\omega_{corr,0}$ and $(P_{dg,i,0}, Q_{dg,i,0}, V_{dg,i,0},)$ at the pivot point
7 Repeat{ // Starting from leaf point ∈ pivot branch
8 Forward sweep using (4) to (14) find load flows in the lines and the voltage magnitude at buses ∈ pivot branch
9 Read connections at the end point (the joint point)
// Starting with branches
10 Forward/backward sweep using (4) to (14) find load flows in all lines and the voltage magnitude at all buses ∈ each branch connected to the end point
11 Forward sweep using (4) to (14) find load flows in the lines and the voltage magnitude at buses ∈ main trunk section
// If more than one main trunk section is connected to an end point, start with the trunk section that has the longest path to the reflection point (determined by the Dijkstra shortest path algorithm) and continue until finishing all sections and reaching the following joint point ∈ main trunk
12 If this joint point is not the reflection point **GOTO 9 Otherwise continue**
Calculate $P_{mismatch,k}, Q_{mismatch,k}$ and
$k \leftarrow k + 1$
Update $\omega_{corr,k}$ according to $P_{mismatch,k}$
$//\Delta\omega_k = -\frac{P_{mismatch,k}\ \Sigma_{Nac} m_{p_i}}{N_{ac}}$, $\omega_k = \omega^* - \Delta\omega_k$
Update V_{pivot} (Pivot) according to $\alpha\ Q_{mismatch,k}$
$//V_{pivot,k} = V_{pivot}{}^* - m_{q_{pivot}}(Q_{pivot,k-1} - \alpha\ Q_{mismatch,k})$
// This α factor is a ratio factor based on the rating of the pivot point DG relative to other DGs, $\alpha = \frac{S_{pivot,max}}{\sum_{i=1}^{Ndg} S_{i,max}}$
} Until ($P_{mismatch,k}$ **AND** $Q_{mismatch,k}$) < tolerance
Calculate voltage angle at all buses using (15)
Display voltages, load flows, frequency, and active/reactive powers

Fig. 4. Pseudo code of the FR-FBS load flow algorithm for the ac subgrid.

2) *Branch sections:* {8-7, 11-10-9-7, 14-13, 21-20-19 and 18-17-16}
3) *Pivot branch section:* {16-17-18}

According to the FR-FBS algorithm outlined in Fig. 4, the directed FR-FBS starts at the pivot point (point 18) and solves toward the reflection point (point 0), as indicated by the arrows in Fig. 5. It then returns to the pivot point after modifying the pivot voltage according to the mismatch in reactive power $Q_{mismatch,k}$. The ac subgrid frequency ω is updated according to the active power mismatch $P_{mismatch,k}$.

In this main forward direction, (4) to (15) are used for calculating $(P_{Loss}Q_{Loss}, P_{flow}, Q_{flow})$ in each section and for computing $(P_{Inj}, Q_{Inj}, V, \delta)$ at each node of the pivot branch and main trunk sections. The voltage is thus updated at all of these nodes based on the pivot point voltage, and the power

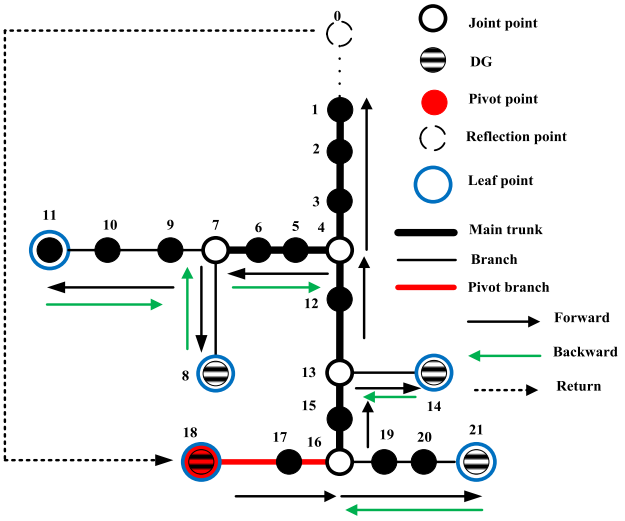

Fig. 5. AC subgrid illustrating the categorization concept and execution steps.

flows are then updated accordingly. At any joint point, an FBS is also executed. The sweep can be divided into two phases:

1) *A forward sweep toward the leaf points:* Equations (4) to (15) are used for calculating $(P_{Loss}, Q_{Loss}, P_{flow}, Q_{flow})$ in each section and $(P_{Inj}, Q_{Inj}, V, \delta)$ at each node of each branch emanating from the joint point.
2) *A backward sweep toward the joint point:* Only values for $(P_{Loss}, Q_{Loss}, P_{flow}, Q_{flow})$ are calculated using (4) to (9). The voltages are thus updated in the forward direction only. However, if a DG unit is connected to a node, the voltage calculated during the forward sweep will update the reactive power injected from the DG unit during the backward sweep using DG's droop characteristics.

For example, in Fig. 5, at node 13 the algorithm executes a forward calculation for node 14 using (V_{13}, δ_{13}) to determine. (V_{14}, δ_{14}). In the backward sweep to node 13, the calculated voltage at node 14 is used to obtain the injected reactive power at node 14 using the DG's droop characteristics. Afterwards, the algorithm will continue the forward calculation from node 13 to node 12 with the power flows calculations accounted for the injections from the DG at node 14. This concept is continued until reaching the reflection point.

At the reflection point, the return calculations are executed. At this stage, the active and reactive power mismatches are calculated and used for updating ω of the ac grid and the voltage at the pivot point, as detailed in the pseudo code shown in Fig. 4. It is noteworthy that the reactive power mismatch calculated at this stage incorporates the effect of reactive power injected from all non-pivot DG's because these injections are considered in the backward sweep calculations. Finally, if the error is not within the specified limit, the algorithm then repeats the process from the main forward sweep.

For the system shown in Fig. 4, the algorithm starts the forward calculations $(P_{Loss}, Q_{Loss}, P_{flow}, Q_{flow}, P_{Inj}, Q_{Inj}, V, \delta)$ from nodes 18-16. At node 16, which is a joint point, an FBS is executed. During the forward sweep from nodes 16-21,

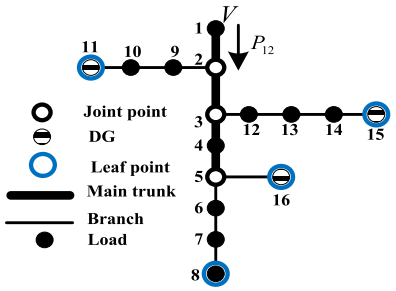

Fig. 6. DC subgrid illustrating the categorization concept.

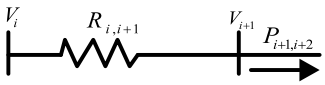

Fig. 7. Simple two-bus dc system.

$(\mathrm{P_{Loss}}, \mathrm{Q_{Loss}}, P_{flow}, Q_{flow}, P_{Inj}, Q_{Inj}, V, \delta)$ are calculated. At the leaf point (node 21), a backward sweep is executed toward the leaf point (node 16). During the backward sweep, only $(\mathrm{P_{Loss}}, \mathrm{Q_{Loss}}, P_{flow}, Q_{flow})$ are calculated using the voltages determined during the forward sweep. At node 16, the algorithm continues its main forward sweep through the main trunk toward node 13, and the steps are then repeated until the reflection point is reached.

A special case occurs when two main trunk sections are connected to a joint point. In such a case, the FR-FBS solution algorithm is directed by Dijkstra's shortest path algorithm. Thus, if two or more main trunk sections are connected, Dijkstra's algorithm calculates the shortest paths to the reflection point. It then determines which section has the longest of the shortest paths to the reflection point and should therefore be calculated first. For example, with respect to solving the main trunk section 13-12-4, at point 4, two main trunk sections are connected: 4-3-2-1 and 4-5-6. The algorithm should start with the section with the longest of the shortest paths to the reflection point, based on the Dijkstra calculation. Since point 5 is farther away than point 3, the FR-FBS algorithm is directed to calculate 4-5-6-7 first.

IV. BFS for a DC Subgrid

The dc subgrid is categorized using terms similar to those previously defined for the ac subgrid. The system nodes are then designated accordingly as either joint, load, or leaf points. The lines are also categorized as main trunk or branches, as shown in Fig. 6. The system is solved through BFS iterations. In the backward sweep calculations, load flows are calculated toward the main trunk, starting from all leaf points. The main trunk is then solved toward the interconnection point.

For the two buses shown in Fig. 7, during the backward sweep, $P_{i+1,i+2}$ and V_{i+1} are known, while $P_{loss\ i+1,i}$ and $P_{i,i+1}$ are calculated using (18) to (20).

$$P_{injected,i+1} = P_{i+1,i+2} + P_{Load,i+1} - P_{gDC,i+1} \tag{18}$$

$$P_{loss\ i+1,i} = R_{i,i+1*}\left(\frac{P_{injected,i+1}}{V_{i+1}}\right)^2 \tag{19}$$

$$P_{i,i+1} = P_{injected,i+1} + P_{loss\ i+1,i} \tag{20}$$

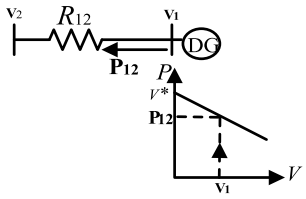

Fig. 8. Leaf point connected to a droop-controlled dc-DG unit.

The forward sweep calculations then start from the interconnection point, which has a constant voltage V. The voltages at all system points are then computed. In the forward sweep, $P_{i,i+1}$ and V_i are known, and V_{i+1} is calculated using (21) and (22).

$$V_{Drop\ i,i+1} = R_{i,i+1*}\left(\frac{P_{i,i+1}}{V_i}\right) \tag{21}$$

$$V_{i+1} = V_i - V_{Drop\ i,i+1} \tag{22}$$

For points connected to leaf points that have droop-controlled DGs, the FBS equations can be modified to account for the DG droop control. For example, in the system shown in Fig. 8, the power balance equation at the DG bus can be written as follows:

$$P_{12} = V_1\left(\frac{V_1 - V_2}{R_{12}}\right) = \frac{V^* - V_1}{m_V} \tag{23}$$

This power balance equation can then be rearranged to calculate the DG bus voltage V_1 as a function of V_2 (voltage at the preceding bus) and the DG droop parameters, as follows:

$$\frac{1}{R_{12}}V_1^2 + \left(\frac{1}{m_V} - \frac{V_2}{R_{12}}\right)V_1 = \frac{V^*}{m_V} \tag{24}$$

Equation (24) is used for the forward sweep voltage calculation, with V_2 known and V_1 unknown. Equation (23) is used in the backward sweep load flow calculation. The FBSs are repeated for the dc subgrid until convergence. At this point, the power fed to the dc subgrid (P_{12}) and the voltage at all dc buses are known.

V. Hybrid AC/DC System

The FBS for solving hybrid ac/dc systems is formulated through the integration of the FR-FBS load flow of the ac subgrid with the FBS load flow of the dc subgrid (Fig. 2). The dc subgrid is represented as an ac DG with constant power $P_{interchange}$ and a $Q - V$ droop. The dc subgrid has a reference bus with a constant voltage V calculated from the ac subgrid frequency (28) [5]. The power balance equations (25) to (29) for the hybrid system are used for relating the ac subgrid frequency to the active power generated in the ac and dc subgrids. The change in ac frequency $\triangle\omega$ is then related to the active power mismatch $\triangle P$, which is calculated at each iteration, as indicated in (30) and (31).

$$P_{g_{AC}} + P_{g_{DC}} = P_{Load} + P_{Loss} = P_T \tag{25}$$

$$P_{g_{AC}} = \sum_{N_{ac}} \frac{\omega_i^* - \omega}{m_{p_i}} = \sum_{N_{ac}} \frac{\omega_i^*}{m_{p_i}} - \frac{N_{ac}\ \omega}{\sum_{N_{ac}} m_{p_i}} \tag{26}$$

Hybrid ac/dc load flow algorithm

1 Neglect active losses and using (25) calculate initial guess of ω
3 Calculate dc voltage V using (28)
4 Perform BFS in the dc distribution subgrid
5 Calculate $P_{interchange}$
6 Perform FR-FBS in the ac subgrid considering the dc link as a DG with constant P and droop-controlled Q
7 Calculate $P_{mismatch}$ and $Q_{mismatch}$
8 Using (31) and $\Delta P = P_{mismatch}$ find $\Delta\omega$ and update ω
9 Using $Q_{mismatch}$ update the pivot voltage
10 GOTO **3** and repeat until convergence

Fig. 9. Pseudo code of the hybrid load flow algorithm.

$$P_{g_{DC}} = \sum_{N_{dc}} \frac{V_i^* - V}{m_{V_i}} = \sum_{N_{dc}} \frac{V_i^*}{m_{V_i}} - \frac{N_{dc}\ V}{\sum_{N_{dc}} m_{V_i}} \tag{27}$$

$$V = \frac{C_\omega \omega + C}{C_V} \tag{28}$$

$$P_{g_{DC}} = \sum_{N_{dc}} \frac{V_i^*}{m_{V_i}} - \frac{N_{dc}\ \frac{C_\omega \omega + C}{C_V}}{\sum_{N_{dc}} m_{V_i}} \tag{29}$$

$$\frac{\partial P}{\partial \omega} = -\frac{N_{ac}}{\sum_{N_{ac}} m_{p_i}} - \frac{N_{dc}\frac{C_\omega}{C_V}}{\sum_{N_{dc}} m_{V_i}} \tag{30}$$

$$\triangle\omega = \frac{\triangle P}{-\frac{N_{ac}}{\sum_{N_{ac}} m_{p_i}} - \frac{N_{dc}\frac{C_\omega}{C_V}}{\sum_{N_{dc}} m_{V_i}}} \tag{31}$$

Fig. 9 shows the pseudo code for the hybrid ac/dc load flow algorithm. This pseudo code delineates the integration of the previously discussed FR-FBS for the ac subgrid with the BFS for the dc subgrid.

It is worth mentioning that if multiple ICs are installed in the same hybrid microgrid, they employ a droop control scheme that allows active power sharing among the ICs. This droop scheme is realized by introducing an intentional error between the normalized voltage and frequency [5]:

$$\mathrm{e_{pu,x}} = \omega_{\mathrm{pu}} - \mathrm{V_{pu,x}} \tag{32}$$

where e is an intentional error introduced between the per unit frequency and dc voltage of the subgrids. This error is a variable that stimulates the ICs to share the active power transfer in proportion to their capacities. The power injected at the ac side is thus expressed as

$$\mathrm{P_{IC,x}} = \frac{1}{K_x}\mathrm{e_{pu,x}} \tag{33}$$

where $\mathrm{P_{IC,x}}$ is the active power injected at the ac side, and $\mathrm{k_x}$ is an error coefficient inversely proportional to the IC capacity. However, proportional power sharing is not guaranteed if the ICs are installed at different dc buses, because, unlike the ac frequency, the dc voltage is not a global power flow variable in dc subgrids.

When these modifications are considered in the modeling of the dc subgrid effect on the ac subgrid frequency, (30) is altered as presented in (34) to account for the error introduced between ω_{pu} and $\mathrm{V_{pu}}$. Hence, (31) is also modified as indicated in (35).

TABLE I
CATEGORIZATION OF AC AND DC SUBGRIDS

	ac subgrid	dc subgrid
Leaf points	A4 and A5	D1, D3, and D5-D7
Joint points	A2	D2 and D4
Branches	A1A4 and A2A5	D3D2, D5D4, D1D2, D6D4, and D7D4
Main trunk	A2A3 and A2A1	D2D4
	Pivot point A6 Reflection point A0 Pivot branch: A6A3	Constant V point: D2

$$\frac{\partial P_{gDC}}{\partial \omega} = \sum_{x=1}^{N_{IC}} \frac{-\left(\frac{C_\omega}{C_V}\right)\sum_{j=1}^{N_{dg,x}} \frac{1}{m_{V,j}}}{1 - \frac{1}{K_x C_V}\sum_{j=1}^{N_{dg,x}} \frac{1}{m_{V,j}}} \tag{34}$$

$$\triangle\omega = \frac{\triangle P}{-\frac{N_{ac}}{\sum_{N_{ac}} m_{p_i}} - \sum_{x=1}^{N_{IC}} \frac{-\left(\frac{C_\omega}{C_V}\right)\ \sum_{j=1}^{N_{dg,x}} \frac{1}{m_{V,j}}}{1-\frac{1}{K_x C_V}\sum_{j=1}^{N_{dg,x}} \frac{1}{m_{V,j}}}}. \tag{35}$$

VI. CASE STUDIES

This section presents several case studies that demonstrate the flexibility of the proposed algorithm. A small-scale hybrid system was first used for detailing the procedure, application, and convergence of the proposed algorithm. The algorithm was then applied for solving the power flow problem of a large-scale power system that includes multiple dc links. The latter case study included a variety of operational scenarios for investigating direct practical applications of the algorithm.

A. Simple 13-Bus System

The simple hybrid system presented in Fig. 10 (a) was used for illustrating the proposed FBS load flow when applied to hybrid ac/dc systems. As shown in Fig. 10 (b), the ac and dc subgrids are first categorized according to the criteria explained in Section III. Table I lists the categorized ac and dc subgrid points and branches.

As indicated in Fig. 9, starting with the load generation balance and neglecting losses, an initial guess for ω is calculated based on (25) to (29). Using (28), the voltage at D2 is computed. This voltage is assumed to be constant, and a BFS is applied in order to solve the dc subgrid for the calculation of the interchange power $P_{interchange}$. The BFS for the dc system begins with the assumption that all points have a voltage V. It then backward calculates the load flow using (18) to (20). The calculation proceeds from the leaf points to the joint points, and then to the main trunk section, until the constant V point (D2) is reached.

The forward calculation phase then starts with the calculation of the voltage at all points, based on (21) to (22). These sweeps are repeated until convergence with respect to point voltage and branch flows. The calculation of power injected at the constant V point (D2) represents $P_{interchange}$. The dc subgrid is thus represented by a DG at A5 that has constant power and droop controlled Q.

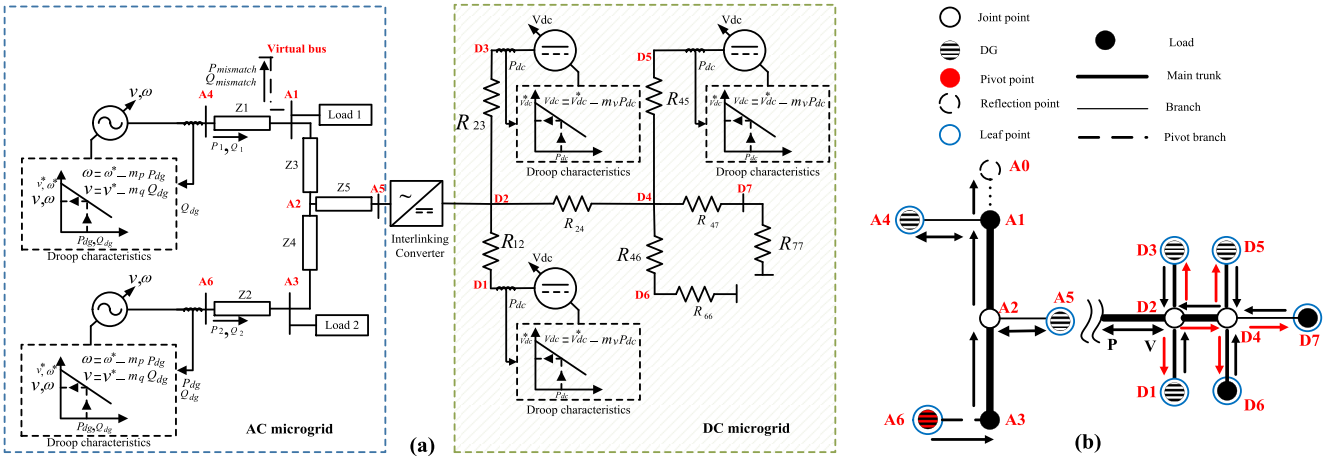

Fig. 10. Simple 13-bus system: (a) ac and dc subgrid schematics; (b) categorization of the subgrids.

TABLE II
LOAD FLOW SOLUTION FOR THE 13-BUS SYSTEM

ac subgrid					dc subgrid		
Bus	$\|V\|$	$\angle\delta$	P_{inj}	Q_{inj}	Bus	V	P_{inj}
A1	0.9704	0.0000	0.0000	0.0000	D1	1.0283	0.3173
A2	0.9933	-0.0071	0.0000	0.0000	D2	1.0252	-0.2719
A3	1.0011	-0.0947	0.0000	0.0000	D3	1.0296	0.3039
A4	1.0282	-0.0099	0.2482	0.1628	D4	1.0218	0.0000
A5	1.0260	0.0086	0.2719	0.0000	D5	1.0231	0.3686
A6	1.0130	-0.1033	0.2482	0.3736	D6	1.0204	0.0000
$\omega = 1.0034\ p.u.$					D7	1.0174	0.0000

The FR-FBS is solved for the ac subgrid starting from the pivot point. The FR-FBS algorithm whose code is provided in Fig. 4 directs the solution, as indicated by the arrows in Fig. 10 (b). At the reflection point (A0), the active and reactive power mismatches $P_{mismatch,k}$ and $Q_{mismatch,k}$ are calculated. Equation (31) is used for computing a new estimate of the frequency ω, which updates the voltage at the dc subgrid for the next dc-BFS iteration. The reactive power mismatch is also used for updating the pivot point voltage for the next ac-FR-FBS.

The results obtained for this 13-bus hybrid system are presented in Table II. As can be seen, the ac DGs share the active power equally because they have the same ratings (i.e., the same slopes) and same frequency. However, they do not share the reactive power equally, due to the unequal voltages at their terminals. In addition, the power injected at A5 represents the power transferred from the dc subgrid to the ac subgrid.

To highlight the robust performance and convergence of the algorithm, a flat start was assumed as the initial system solution. This assumption means that the voltage magnitudes and angles are, respectively, ones and zeros for the system load buses, with no power injection by the droop-controlled DG units. Thus, the DG voltage is V^* (reference voltage) and the ac-subgrid frequency is ω^*.

The pivot-point voltage and the reactive power mismatch shown in Fig. 11 (a) illustrate the convergence of the solution for the pivot-point voltage while the reactive power

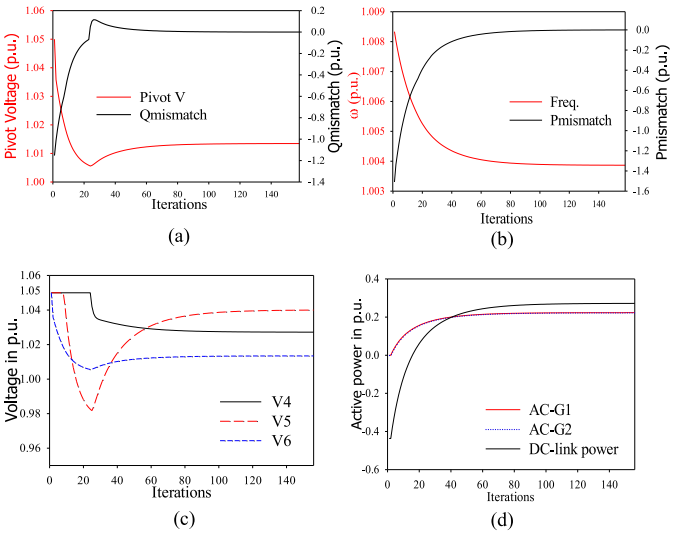

Fig. 11. Convergence of system variables: (a) pivot point voltage and reactive power mismatch; (b) ac subgrid's frequency and active power mismatch; (c) ac DG bus voltages; (d) ac DG active power and dc link power.

mismatch is reaching zero. Similarly, Fig. 11 (b) provides the convergence of the ac-subgrid frequency with the number of iterations as the active power mismatch approaches zero.

With the flat start, all DG voltages start from V^*, and all DG power starts from zero, as can be noted in Fig. 11 (c) and 11 (d). As well, the dc link starts as a load with its power calculated from the application of the flat start in the dc subgrid. It should be noted that the ac DG bus voltages (equivalently, the reactive power injected from the DGs) are bounded, i.e., $V_{min} \leq V_{dg} \leq V_{max}$ (equivalently, $Q_{min} \leq Q_{dg} \leq Q_{max}$). This limitation explains the saturation in the first iterations of V4 and V5 in Fig. 11 (c).

A better starting point can be estimated by neglecting losses and using (25) to find an initial guess for ω, as mentioned in the pseudo code presented in Fig. 9. However, in the simulation discussed in this section, the conventional flat start was used to prove the robustness of the proposed algorithm.

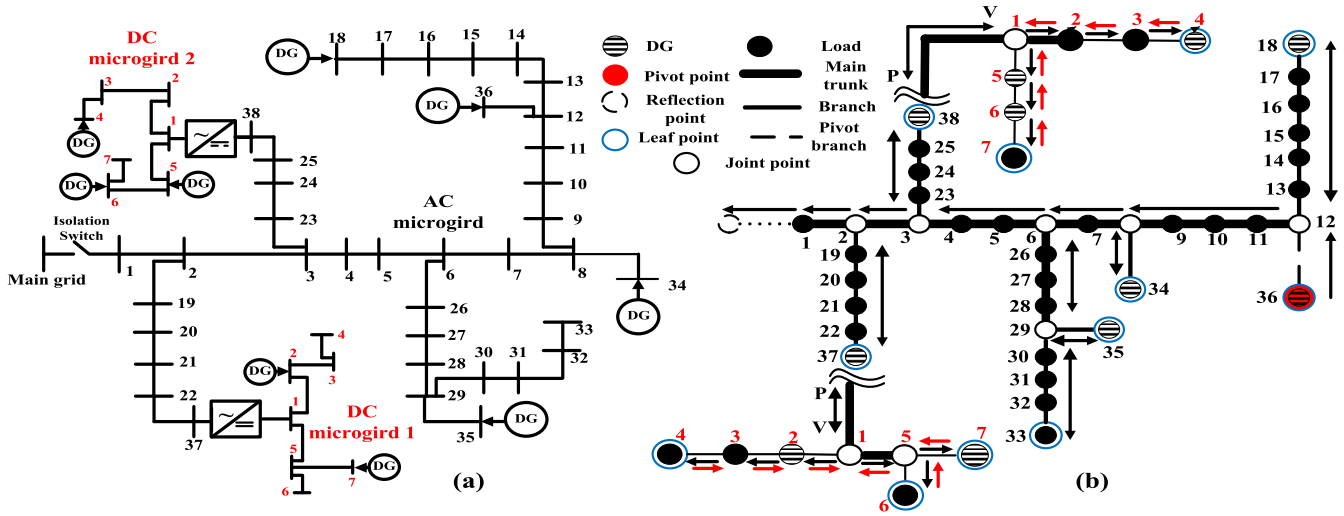

Fig. 12. Multiple ac and dc microgrid layouts for the case studies: (a) ac and dc subgrid schematics; (b) categorization of the subgrids.

B. Multiple AC and DC Microgrids

The successful operation of islanded microgrids has been assessed through several operational studies. Voltage assessment, the effect of IC outages, and the probabilistic load flow in the presence of renewable DGs are considered the most salient studies. As illustrated in Fig. 12 (a), an extended IEEE 38-bus [20] ac microgrid was augmented with two seven-bus dc microgrids. The categorization of the system nodes and branches is shown in Fig. 12 (b). This system was used for highlighting the application of the proposed load flow approach with respect to a number of scenarios chosen to illustrate the performance of these crucial analyses.

1) Effect of Changing the Load Level on the AC Side: This study is essential for assessing the system voltage profile as well as the power sharing behavior when the system loading level λ is changed. These indicators are used for determining the maximum loadability of the system or any further readjustment required in the DG droop characteristics in order to avoid overloading.

The analysis for this scenario addresses system performance with respect to the possibility of changing the value of λ from 70 % to 150 %. As revealed in Fig. 13, according to conventional droop settings, the system voltage profile is within the limit up to 150 % of the loading level. Beyond this value of λ, the system exhibits an under-voltage condition at bus 33. This situation could be handled through further OPF studies similar to those reported in [21], but such studies are beyond the scope of this work.

However, the DG unit at bus 34 was tested at different candidate locations in order to examine the impact on the voltage regulation when the DG location is changed. The DG unit was allocated at buses (1, 3, and 6), and the voltage profiles obtained are presented in Fig. 13. As indicated in the figure, reallocating the DG unit to bus 6 avoids the voltage violation, and the voltage profile is retained within normal limits. On the other hand, as shown in Fig. 14, due to the excellent sharing characteristics provided by (3), droop settings result in highly appropriate sharing among all DG units in both the ac and dc subgrids.

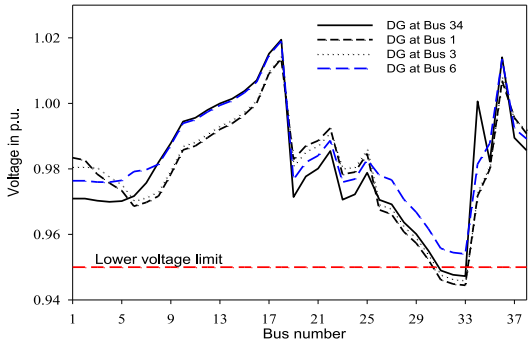

Fig. 13. Voltage profiles for a variety of DG locations for $\lambda = 150\%$.

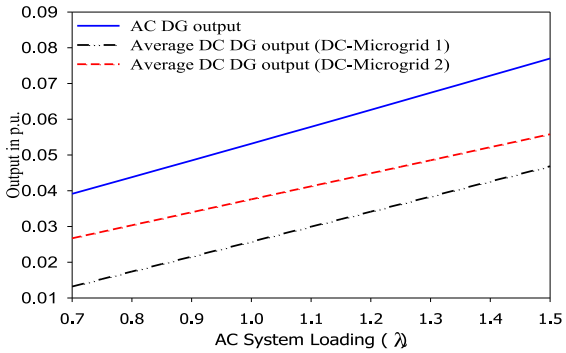

Fig. 14. Power sharing between ac and dc DGs.

2) Effect of IC Outage: It is important to recall that the main IC objective is to facilitate active power sharing among the ac and dc subgrids. In this regard, several operational characteristics have been suggested in the literature. For example, Abdelaziz *et al.* [21] proposed active power transfer through an IC using active and reactive power reference values that are updated according to a centralized supervisory control. Another operational strategy based on the application of the coupling approach has been investigated for the current study and is expressed in (3). It relies on local information for the updating of the active power transfer, even with a delayed supervisory control signal. To show the flexibility of the

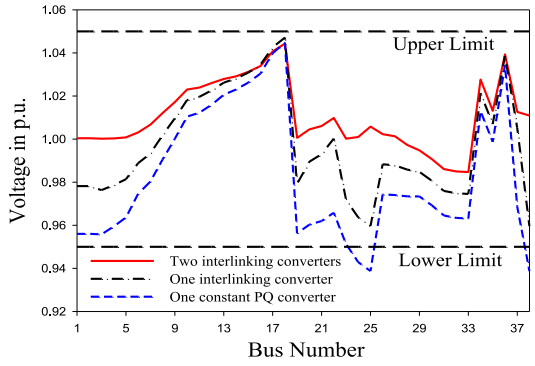

Fig. 15. Voltage profiles for a variety of dc converter modes of operation.

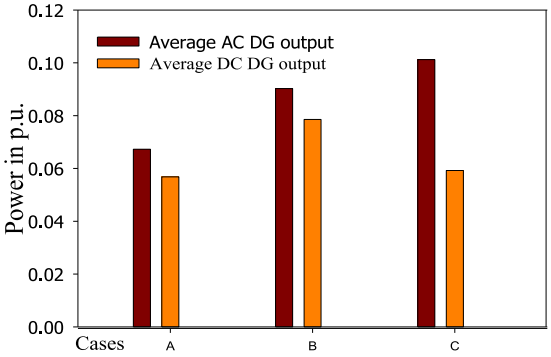

Fig. 16. Average DG power for a variety of dc converter modes of operation.

proposed algorithm, the application of both control schemes for a case study involving an outage of IC #2 was examined. Three different scenarios were investigated. The first scenario (Case A) involves the two system ICs that remain in healthy working order. The other two scenarios were focused on system performance after an outage of IC #2 during the implementation of either coupling characteristics (Case B) or constant PQ characteristics (Case C). Fig. 15 presents the voltage profile for the three cases. As indicated, the interlinking operation mode allowed the dc microgrid to support the ac microgrid voltage after the other dc microgrid was disconnected, which helped keep the voltage within allowable limits. An additional effect is that, in interlinking operation mode, the power supplied from the disconnected dc microgrid was dispatched between the generators in the ac and dc microgrids.

Fig. 16 shows the average DG power in the ac and dc microgrids for the three cases. In interlinking operation mode (Case B), the average power ratio was kept almost the same as that in Case A. In contrast, for Case C, a large increase in the average DG power was evident in the ac microgrid when one of the dc microgrids was disconnected.

The frequency deviations from 60 Hz for the three different cases are displayed in Table III. The results show how the interlinking operation mode supports the ac system frequency when the load increases following the disconnection of one of the dc microgrids.

3) Probabilistic Load Flow in the Presence of Renewable DGs and With Consideration of the Probabilistic Load Profile: Renewable-based generators are becoming key components

TABLE III
FREQUENCY DEVIATIONS FOR DC CONVERTER MODES OF OPERATION

	Case A	Case B	Case C
Δf in Hz	0.3060	0.5020	0.7140

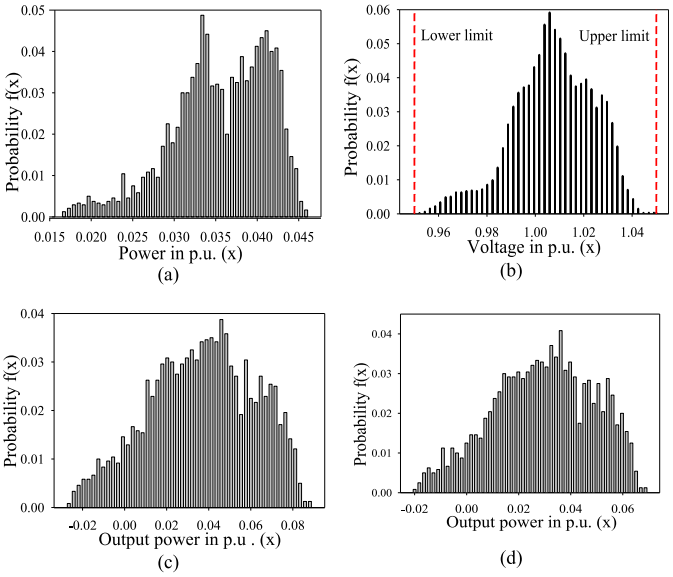

Fig. 17. PDFs for a variety of variables during summer: (a) power interchange; (b) ac subgrid bus voltages; (c) average ac output power in the ac subgrid; (d) average DG output power in the dc subgrid.

of the microgrid supply mix. This category of generators is weather dependent and therefore highly probabilistic in nature. To be effective, a tool for evaluating the performance of microgrid operation should be capable of taking such probabilistic behavior into account. The developed hybrid load flow has therefore been integrated with a probabilistic load and generation model to create a probabilistic load flow tool for use with hybrid islanded microgrids.

To verify the efficacy of this tool, for the system depicted in Fig. 12, two wind-based generators are assumed to be connected at buses 18 and 38 of the ac microgrid. Two solar-based generators are also assumed to be part of the dc microgrids: one at bus 2 in the first dc microgrid and another at bus 5 in the second. The probabilistic model presented in [22] was adopted for modeling the renewable generation and load. A Monte Carlo simulation (MCS) was employed for determining the probabilistic load flow of the islanded hybrid microgrid.

PDFs of the variables obtained for summer and winter are presented in Fig. 17 and Fig. 18, respectively. The probabilistic loading of the IC during these two seasons is shown in Fig. 17 (a) and Fig. 18 (a). During the winter, due to the substantial amount of wind power located in the ac subgrid and the almost-zero solar power during the evenings, power is transferred from the ac to the dc subgrid. In contrast, during sunny and infrequent-wind-gust periods, power is transferred from the dc to the ac subgrid, hence negatively skewing the power.

On the other hand, the high degree of solar power located in the dc subgrid during the summer keeps the power transfer flowing from the dc to the ac subgrid, creating a positive skew

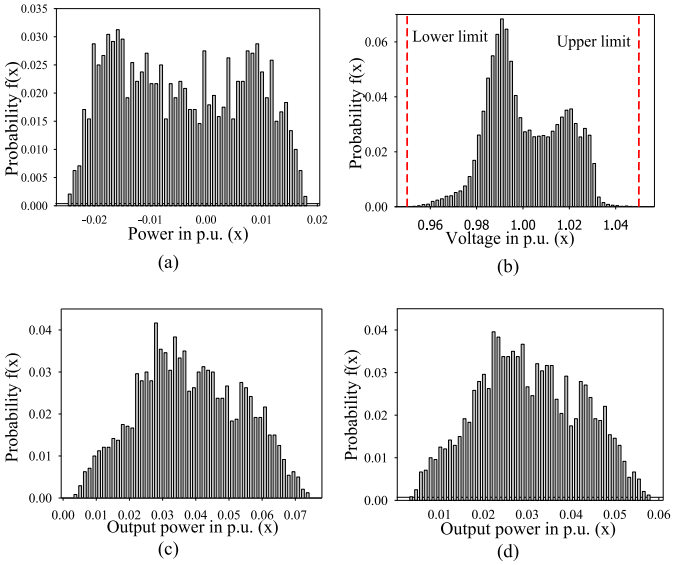

Fig. 18. PDFs for a variety of variables during **winter**: (a) power interchange; (b) ac subgrid bus voltages; (c) average DG output power in the ac subgrid; (d) average DG output power in the dc subgrid.

TABLE IV
RESULTS WITH/WITHOUT THE INTENTIONAL ERROR IN THE IC EQUATION

	Case I (ω_{pu}=0.9949)		Case II(ω_{pu}=0.9948)	
	dc-microgrid 1	dc-microgrid 2	dc-microgrid 1	dc-microgrid 2
$V\ (p.u.)$	0.9827	0.9827	0.9838	0.9824
$e\ (p.u.)$	0	0	-0.0289	0
$P_{interchange}(p.u.)$	0.5979	1.2476	0.5779	1.2551

in the power transfer PDF for that season. The probabilistic voltage at the ac subgrid buses is presented in Fig. 17 (b) and Fig. 18 (b). The results show that the voltage is kept within allowable limits for the range of variations in renewable generation and load power. The effectiveness of the proposed tool for the probabilistic study of isolated hybrid microgrids is thus confirmed.

However, if a violation were to occur, the tool could be used for calculating the power curtailed in order to retain the voltage within permissible limits. The probabilistic average loading of the ac and dc DGs during the two seasons is presented in Fig. 17 (c), Fig. 17 (d), Fig. 18 (c), and Fig. 18 (d). The DG loading in the ac and dc subgrids is correlated due to the coupled frequency and voltage achieved by the IC.

4) Parallel ICs With Introduced Error: In this case study, the first dc microgrid is assumed to be connected through two identical parallel ICs. An intentional error is introduced between ω_{pu} and V_{pu}. In this case, both ICs are assumed to have the same rating, with an equal error coefficient $k = 0.1$ (i.e., $k_{equivalent} = 0.05$). To execute the hybrid load flow algorithm and account for the error introduced into the IC equation (32), the pseudo code presented in Fig. 9 is modified as shown in Fig. 19. Table IV indicates the results for both cases: with no error and when the error between the normalized voltage and frequency is introduced.

1 Knowing ω_{pu} assuming e_{pu}=0
2 $V_{pu} = \omega_{pu} - e_{pu}$
3 BFs in the dc subgrid with V=V_{pu} and calculate P_{total} at convergence
4 Using P_{total} update $e_{pu} = k_{equivalent}\ P_{total}$
5 GOTO 2 while $\Delta e_{pu} > \varepsilon$
6 Calculate $P_x = \frac{1}{k_x} e_{pu}$
7 Perform FR-FBS in the ac subgrid considering the dc link as a DG with constant P and droop-controlled Q
8Calculate $P_{mismatch}$ and $Q_{mismatch}$
9 Using (35) and $\Delta P = P_{mismatch}$ find $\Delta\omega$ and update ω
10 Using $Q_{mismatch}$ update the pivot voltage
11 GOTO **1** and repeat until convergence

Fig. 19. Pseudo code of the hybrid load flow algorithm including the error introduced to all parallel IC operation.

VII. CONCLUSION

A novel branch-based load flow algorithm has been presented for the steady-state analysis of islanded hybrid microgrids. The proposed algorithm divides the load flow of the hybrid system into two coupled subproblems that are solved sequentially. Branch-based algorithms have been developed for the ac and dc subgrids and then integrated based on the IC characteristics in order to form the proposed load flow tool.

The developed algorithm is derivative free and overcomes the challenges associated with the application of branch-based algorithms for isolated hybrid microgrids. It has been explained in detail and illustrated through its implementation for a simple hybrid system. Its generalization and application for a modified IEEE 38-bus system have also been presented.

The algorithm has been proven to be highly suitable for performing numerous steady-state analyses. The analyses examined include the effects of load variation, a variety of IC control strategies, and the probabilistic nature of the impact of renewable resources and loads on system performance. The simplicity of the developed algorithm and its minimal computational requirements represent crucial advantages that could facilitate its practical implementation in future hybrid microgrids.

It should be noted that the three-phase balanced case (or positive sequence solution) was considered in the study as proof of concept. The overall objective of the proof of concept was to find solutions to the technical challenges associated with the application of branch-based techniques to islanded hybrid microgrids. These challenges include the execution of the FB and BF sweeps, the treatment of the DC subgrid as an integrated part of the ac load flow, and guaranteeing the convergence of the method.

The positive sequence solution is, in fact, the building block for load flow analysis using the sequence components, as presented in [23]. The work presented in this paper thus constitutes an important preliminary exploration. However, its extension to include unbalanced load flow is not trivial. The authors' future work will therefore entail the full inclusion

TABLE V
WIND MODELS

Model	W1	W2	W3	W4
Season	Spring	Fall	Summer	Winter
γ	0.40832	0.1866	0.48423	-0.0199
δ	0.46673	0.49059	0.55561	0.48906
λ	0.97881	0.98015	0.97956	0.95746
ζ	-0.0765	-0.00616	-0.00874	0.005568

TABLE VI
SOLAR MODELS

Model	S1	S2	S3	S4	S5
Season	Spring (5h-20h)	Fall (5h-20h)	Summer (5h-20h)	Winter (5h-20h)	Other
γ	0.0925	0.1635	-0.18985	0.4452	No output power (P = 0)
δ	0.47215	0.44444	0.61823	0.47877	
λ	0.7118	0.6483	0.63197	0.731273	
ζ	0.92239	0.39591	0.79265	0.28251	

of unbalanced cases in the analysis in order to determine necessary modifications

APPENDIX

A. Load and Generation Probabilistic Models

The probabilistic models used for load and renewable generation are based on the models provided in [22]. The following are the details of these models.

1) *Wind-Based Generation Modeling:* To accurately model the power output from wind-based generators, real historical wind-speed data for three successive years at a specific site are converted into output power using wind energy conversion system (WECS) characteristics. With P_{rated} considered as 1 p.u., the wind speed is now converted into p.u. output power with the power base equal to the rated power of the wind-based generator. These historical p.u. powers are then clustered into four clusters (scenarios) representing the four seasons. For each cluster, the best-fit PDF for all the p.u. power data belonging to that cluster is used for modeling the output power from the wind-based DGs. Goodness-of-fit tests are employed for a determination of the best PDF. In this case, the Johnson SB expressed in (36) and (37) was found to be the best-fit PDF for the wind data.

$$\mathrm{f(x)} = \frac{\delta}{\lambda\sqrt{2\pi}\mathrm{z}(1-\mathrm{z})}\exp\left(-\frac{1}{2}\left(\gamma+\delta\ln\left(\frac{\mathrm{z}}{1-\mathrm{z}}\right)\right)^2\right) \tag{36}$$

$$z \equiv \frac{x-\xi}{\lambda} \tag{37}$$

The model parameters for the different seasons are presented in Table V.

2) *Solar-Based Generation Modeling:* The same modeling approach used for the wind data is adopted for three successive years of historical solar-irradiance data at the same site. The data are used for calculating the p. u. solar output power. The p.u. data obtained are examined in order to select the best-fit PDF that models the p.u. solar output power. As with the wind modeling, the year is divided into four seasons. For each season, only the non-zero power periods are considered. In this case, the Johnson SB described by equations (36) and (37) was found to represent the best-fit PDF. The parameters of the Johnson SB PDF that models each season (S1-S4) are indicated in Table VI. Hence, solar power is modeled using five models (S1-S5), with S5 modeling zero output (for periods outside the 5 h to 20 h window).

TABLE VII
LOAD MODELS

Season	Day	Model	α	β	γ
Spring	weekday	L1	2.4226	0.09934	-0.08812
	weekend	L2	1.7979	0.05353	-0.04758
Fall	weekday	L3	5.247	0.22676	-0.20872
	weekend	L4	5.1698	0.16188	-0.14876
Summer	weekday	L5	8.2088	0.21547	-0.20307
	weekend	L6	17.046	0.29313	-0.28402
Winter	weekday	L7	8.2088	0.21547	-0.20307
	weekend	L8	17.046	0.29313	-0.28402

3) *Load Modeling:* The load model is obtained using the IEEE-RTS [24] load profiles. These load profiles are clustered into eight clusters (4 seasons × 2 days per season), as presented in Table VII. Each cluster is modeled with the centroid of the cluster as a deterministic load profile. A random error is added to the determinstic load profile of each cluster to account for the probablistic behavior of the load. This error is obtained by selecting the best-fit PDF to model the error data calculated for each cluster, as explained in [22].

The Weibull PDF expressed in (38) is the best-fit PDF used for modeling the error associated with each cluster centroid. The PDF parameters for each cluster are shown in Table VII.

$$f(x) = \frac{\alpha}{\beta}\left(\frac{x-\gamma}{\beta}\right)^{\alpha-1} e^{-\left(\frac{x-\gamma}{\beta}\right)^{\alpha}}. \tag{38}$$

B. Monte Carlo Simulation

The MCS process consists of four steps, as detailed in Fig. 20. Step 1, which is the modeling of the input variables, is adopted from [22], as explained in the previous section. These input variables are the renewable generation and load powers. In the models obtained, these random variables are represented by continuous PDFs, as required for the application of the MCS. The sampling of random variables (step 2) is presented below. The numerical experimentation (step 3) is the power flow technique presented in this paper. Samples of the output variable, which is the power flow solution in our study, constitute the output from setp 3. In the final step, step 4, the output is analyzed in order to investigate its probabilistic characteristics.

The sampling process, step 2, used for producing samples of generation and load PDFs, is carried out as follows.

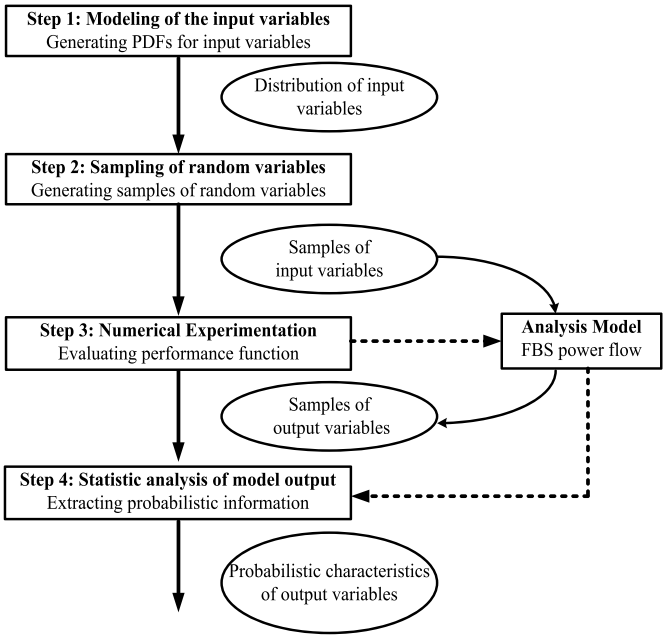

Fig. 20. Monte Carlo simulation process.

1) MCS Samples for the Weibull Distribution: As explained earlier, the load is modeled with a Weibull PDF with parameters (α, β, γ), as expressed in equation (38). The general steps for generating samples from a PDF are as follows:

- $f(x) \leftarrow F(x)$: Convert the PDF into a cumulative density function (CDF).
- $f(x) \leftarrow F^{-1}(x)$: Compute the inverse CDF.
- $u \leftarrow U \in [0, 1]$: Generate sample u from the uniform distribution on [0, 1].
- $x = F^{-1}(u)$: Find the required sample x using the inverse CDF.

To generate a random sample from a Weibull distribution, the inverse CDF for the Weibull distribution is first found, as follows:

$$F(x) = 1 - e^{\left[-\left(\frac{x-\gamma}{\beta}\right)^{\alpha}\right]} \tag{39}$$

The pseudo code presented in Fig. 21 [25] is then used for generating M random samples x from the Weibull distribution, following the general steps explained previously.

2) MCS Samples for the Johnson SB Distribution: Following the general steps for generating samples from a Johnson SB PDF is complicated. It is thus essential to present simple steps that can be used to carry out the MCS for the Johnson SB distribution. For this reason, another approach is used for the Johnson SB PDF, whereby the distribution is related to a normal distribution through a bounded transformation T(x), as follows:

$$z = \gamma + \delta T(x) \tag{40}$$

where transformation T(x) for the Johnson SB distribution is defined as

$$T(x) = \ln\left(\frac{x-\zeta}{\lambda+\zeta-x}\right) \tag{41}$$

For i = 1: M
Generate Uniform (0,1) → R
Calculate $x = \gamma + \beta\,(-\ln(1-R))^{\frac{1}{\alpha}}$
End

Fig. 21. Algorithm used for generating random samples from Weibull PDF.

For i = 1: M
Generate Normal (0,1) → R
Calculate $E = e^{\frac{R-\gamma}{\delta}}$
Calculate $x = \zeta + \lambda\left(\frac{E}{1+E}\right)$
End

Fig. 22. Algorithm used for generating random samples from Johnson SB PDF.

Based on (40) and (41), the algorithm required for performing the MCS for the Johnson SB PDF with parameters (δ, λ, γ, ζ) is as shown in Fig. 22 [25]. This algorithm generates M random samples x from the Johnson SB PDF through the transformation of a normal random variable R to a Johnson SB random variable x.

REFERENCES

[1] T.-F. Wu, "Guest editorial—Special issue on power electronics in DC distribution systems," *IEEE Trans. Power Electron.*, vol. 28, no. 4, pp. 1507–1508, Apr. 2013.
[2] L. Che and M. Shahidehpour, "DC microgrids: Economic operation and enhancement of resilience by hierarchical control," *IEEE Trans. Smart Grid*, vol. 5, no. 5, pp. 2517–2526, Sep. 2014.
[3] H. M. A. Ahmed, A. B. Eltantawy, and M. M. A. Salama, "A planning approach for the network configuration of AC–DC hybrid distribution systems," *IEEE Trans. Smart Grid*, to be published.
[4] J. M. Guerrero, J. C. Vasquez, J. Matas, L. G. de Vicuna, and M. Castilla, "Hierarchical control of droop-controlled AC and DC microgrids—A general approach toward standardization," *IEEE Trans. Ind. Electron.*, vol. 58, no. 1, pp. 158–172, Jan. 2011.
[5] P. C. Loh, D. Li, Y. K. Chai, and F. Blaabjerg, "Autonomous operation of hybrid microgrid with AC and DC subgrids," *IEEE Trans. Power Electron.*, vol. 28, no. 5, pp. 2214–2223, May 2013.
[6] N. Eghtedarpour and E. Farjah, "Power control and management in a hybrid AC/DC microgrid," *IEEE Trans. Smart Grid*, vol. 5, no. 3, pp. 1494–1505, May 2014.
[7] P. C. Loh, D. Li, Y. K. Chai, and F. Blaabjerg, "Autonomous control of interlinking converter with energy storage in hybrid AC–DC microgrid," *IEEE Trans. Ind. Appl.*, vol. 49, no. 3, pp. 1374–1382, May/Jun. 2013.
[8] M. M. A. Abdelaziz and E. F. El-Saadany, "Maximum loadability consideration in droop-controlled islanded microgrids optimal power flow," *Elect. Power Syst. Res.*, vol. 106, pp. 168–179, Jan. 2014.
[9] C. S. Cheng and D. Shirmohammadi, "A three-phase power flow method for real-time distribution system analysis," *IEEE Trans. Power Syst.*, vol. 10, no. 2, pp. 671–679, May 1995.
[10] S. M. Moghaddas-Tafreshi and E. Mashhour, "Distributed generation modeling for power flow studies and a three-phase unbalanced power flow solution for radial distribution systems considering distributed generation," *Elect. Power Syst. Res.*, vol. 79, no. 4, pp. 680–686, Apr. 2009.
[11] A. B. Eltantawy and M. M. A. Salama, "A novel zooming algorithm for distribution load flow analysis for smart grid," *IEEE Trans. Smart Grid*, vol. 5, no. 4, pp. 1704–1711, Jul. 2014.
[12] M. M. A. Abdelaziz, H. E. Farag, E. F. El-Saadany, and Y. A.-R. I. Mohamed, "A novel and generalized three-phase power flow algorithm for islanded microgrids using a newton trust region method," *IEEE Trans. Power Syst.*, vol. 28, no. 1, pp. 190–201, Feb. 2013.
[13] A. Cataliotti *et al.*, "An innovative measurement approach for load flow analysis in MV smart grids," *IEEE Trans. Smart Grid*, vol. 7, no. 2, pp. 889–896, Mar. 2016.

[14] D. Shirmohammadi, H. W. Hong, A. Semlyen, and G. X. Luo, "A compensation-based power flow method for weakly meshed distribution and transmission networks," *IEEE Trans. Power Syst.*, vol. 3, no. 2, pp. 753–762, May 1988.
[15] G. Gross and H. W. Hong, "A two-step compensation method for solving short circuit problems," *IEEE Power Eng. Rev.*, vol. PER-2, no. 6, pp. 22–23, Jun. 1982.
[16] G. Díaz, J. Gómez-Aleixandre, and J. Coto, "Direct backward/forward sweep algorithm for solving load power flows in AC droop-regulated microgrids," *IEEE Trans. Smart Grid*, vol. 7, no. 5, pp. 2208–2217, Sep. 2016.
[17] A. A. Hamad, M. A. Azzouz, and E. F. El Saadany, "A sequential power flow algorithm for islanded hybrid AC/DC microgrids," *IEEE Trans. Power Syst.*, vol. 31, no. 5, pp. 3961–3970, Sep. 2016.
[18] A. A. Eajal, M. A. Abdelwahed, E. F. El-Saadany, and K. Ponnambalam, "A unified approach to the power flow analysis of AC/DC hybrid microgrids," *IEEE Trans. Sustain. Energy*, vol. 7, no. 3, pp. 1145–1158, Jul. 2016.
[19] D. Joyner, M. Van Nguyen, and N. Cohen, *Algorithmic Graph Theory.* 1991. [Online]. Available: http://code.google.com/p/graph-theory-algorithms-book/EditionVersion 0.62011 January 06
[20] D. Singh, R. K. Misra, and D. Singh, "Effect of load models in distributed generation planning," *IEEE Trans. Power Syst.*, vol. 22, no. 4, pp. 2204–2212, Nov. 2007.
[21] M. M. A. Abdelaziz, H. E. Farag, and E. F. El-Saadany, "Optimum droop parameter settings of islanded microgrids with renewable energy resources," *IEEE Trans. Sustain. Energy*, vol. 5, no. 2, pp. 434–445, Apr. 2014.
[22] M. E. Nassar and M. M. A. Salama, "Adaptive self-adequate microgrids using dynamic boundaries," *IEEE Trans. Smart Grid*, vol. 7, no. 1, pp. 105–113, Jan. 2016.
[23] M. Abdel-Akher, K. M. Nor, and A. H. A. Rashid, "Improved three-phase power-flow methods using sequence components," *IEEE Trans. Power Syst.*, vol. 20, no. 3, pp. 1389–1397, Aug. 2005.
[24] T.-F. Wu, "IEEE reliability test system—A report prepared by the reliability test system task force of the application of probability methods subcommittee," *IEEE Trans. Power App. Syst.*, vol. PAS-98, no. 6, pp. 2047–2054, Nov./Dec. 1979.
[25] E. McGrath and D. Irving, *Techniques for Efficient Monte Carlo Simulation. Volume II. Random Number Generation for Selected Probability Distributions.* U.S. Nat. Tech. Inf. Service, 1973.
E. McGrath and D. Irving, *Techniques for Efficient Monte Carlo Simulation. Volume II. Random Number Generation for Selected Probability Distributions*, U.S. Dept. Commerce, Nat. Tech. Inf. Service, Springfield, VA, USA, 1973.

Mohammed Elsayed Nassar (S'06) was born in Alexandria, Egypt, in 1984. He received the B.Sc. and M.Sc. degrees (Hons.) in electrical engineering from Alexandria University, Alexandria, in 2006 and 2010, respectively, and the Ph.D. degree in electrical and computer engineering from the University of Waterloo, Waterloo, ON, Canada, in 2017.

He is currently a part-time Lecturer with the Department of Electrical and Computer Engineering, University of Waterloo. His research interests include electrical machines and drives, distributed and renewable generation, self-healing, smart microgrids, and smart distribution systems.

Amr A. Hamad (S'13) was born in Suez, Egypt, in 1985. He received the B.Sc. (Hons.) and M.Sc. degrees in electrical engineering from Cairo University, Giza, Egypt, in 2007 and 2010, respectively, and the Ph.D. degree in electrical and computer engineering from the University of Waterloo, Waterloo, ON, Canada, in 2016.

He is currently a Research Associate with Measurement Sciences and Standards, National Research Council Canada. His research interests include planning of distribution systems, distributed and renewable generation, control of smart distribution systems, and the development of measurement techniques and instrumentation for accurate measurements of high-voltage active/reactive power and energy under difficult operating conditions.

M. M. A. Salama (F'02) received the B.Sc. and M.Sc. degrees in electrical engineering from Cairo University, Cairo, Egypt, in 1971 and 1973, respectively, and the Ph.D. degree from the University of Waterloo, Waterloo, ON, Canada, in 1977.

He is currently a Professor with the Department of Electrical and Computer Engineering, University of Waterloo. He has consulted widely with governmental agencies and the electrical industry. His research interests include the operation and control of distribution systems, smart microgrids, power-quality monitoring and mitigation, asset management, and electromagnetics. He is a Registered Professional Engineer in the province of Ontario.

Ehab F. El-Saadany was born in Cairo, Egypt, in 1964. He received the B.Sc. and M.Sc. degrees in electrical engineering from Ain Shams University, Cairo, Egypt, in 1986 and 1990, respectively, and the Ph.D. degree in electrical engineering from the University of Waterloo, Waterloo, ON, Canada, in 1998.

He is currently a Professor in the Department of Electrical and Computer Engineering, University of Waterloo. His research interests include smart grid operation and control, microgrids, self healing, power quality, distributed generation, power electronics interfacing, and mechatronics. He is the Canada Research Chair in Smart Distribution Systems, an Editor of the IEEE TRANSACTIONS ON SMART GRID, and a Registered Professional Engineer in the province of Ontario.